Optical Engineering

OpticalEngineering.SPIEDigitalLibrary.org

Aberration properties of odd-order surfaces in optical design

Takao Tanabe
Masato Shibuya

SPIE.

Takao Tanabe, Masato Shibuya, "Aberration properties of odd-order surfaces in optical design," *Opt. Eng.* **55**(12), 125107 (2016), doi: 10.1117/1.OE.55.12.125107.

Aberration properties of odd-order surfaces in optical design

Takao Tanabe[a,b,*] and Masato Shibuya[a]
[a]Tokyo Polytechnic University, Faculty of Engineering, 1583 Iiyama, Atsugi-shi, Kanagawa, 243-0297, Japan
[b]Hakuto Corporation, Design and Development Section, Electric Equipment Division, 1-13, Shinjuku 1-Chome, Shinjuku-Ku, Tokyo 160-8910, Japan

Abstract. We theoretically represent the effectiveness of the odd-order surface for optical designs via an aberration theory. The theory employs an expression of the odd-order surface with aberration coefficients, which are derived by power-series expansion of wavefront aberration with respect to the coordinates of optical surfaces. This expression allows us to understand the aberration characteristics of odd-order surfaces. By applying this aberration theory to the design of extreme ultraviolet lithography optics, we show that odd-order surfaces are effective in reducing higher-order aberrations with fewer coefficients than even-order surfaces do. [DOI: 10.1117/1.OE.55.12.125107]

Keywords: Seidel aberration; odd-order aspherical surface; extreme ultraviolet lithography projection optics.

Paper 161262 received Aug. 10, 2016; accepted for publication Dec. 5, 2016; published online Dec. 28, 2016.

1 Introduction

The usefulness of odd-order surfaces is widely recognized nowadays because the odd-order surface contains odd-order powers of radial coordinate unlike conventional aspherical surfaces and thus provides new degrees of freedom in optical design. A pioneering application of the odd-order surface is found in viewfinder design of instant cameras,[1] for which the odd-order surface plays a major role in correction of astigmatism induced by the tilted curved mirror. The odd-order surface has been applied to imaging optics, such as a projection display[2] and a zoom lens.[3] This surface type has been also applied to lithographic projection systems,[4] in which diffraction-limited imaging performance is required.

Few studies have been performed on odd-order surfaces. Since odd-order surfaces consist of powers of absolute value of radial coordinates, they are rotationally invariant. Thus, one might infer that odd-order surfaces can be expressed as the form of ordinary aspherical surface (even-order power series). However, by considering the differentials of odd-order surfaces, Shibuya et al.[5] proved that odd-order surfaces cannot be represented as an even-order power series. (This is due to the fact that the higher-order differentials of odd-order surfaces cannot be defined at the origin.) This property implies that odd-order surfaces have aberration characteristics different from those of ordinary even-order surfaces. Thus, they concluded that the odd-order surfaces are effective and practically confirmed that odd-order coefficients are effective parameters in optical design. However, this result seems to be contradictory with the completeness of Zernike polynomials because the rotational invariant terms of Zernike polynomials consist only of even-order monomials. Also, the fact that odd-order surfaces can be exactly represented by Zernike polynomials has not been proven. To resolve these problems, Tanabe et al.[6] proved that not only the displacement but also slopes of odd-order surfaces are exactly represented by a finite number of Zernike polynomials. As a result, odd-order surfaces are exactly represented by a finite number of even-order polynomials. (Note that the impossibility of Taylor expansion, which means expansion of odd-order aspherical terms into even-order power series, is not contradictory with the completeness of Zernike polynomials.) They also practically confirmed that the effectiveness of this approximation for the case of Schmidt corrector plate with odd-order terms. However, since the required number of even-order terms, which closely approximates an odd-order surface, is not necessarily realistic for some cases, odd-order surfaces are effective in optical design. To analyze the characteristics of odd-order surfaces, we construct an aberration theory for odd-order surfaces in this paper. Moreover, we study how best to use them for optical design of extreme ultraviolet lithography (EUVL) cameras.

One major derivation of aberration coefficients involves expanding a wavefront function into a power series of pupil coordinates.[7–13] In Sec. 2, following this conventional method, we derive the aberration coefficients of odd-order surfaces to clarify the usefulness of these surfaces. An aspherical ray trace procedure provides a conversion of aspherical sag into additional optical path length and then gives expansion of wavefront aberrations.

Section 3 shows a design example for EUVL cameras with odd-order surfaces, whereas conventional EUVL camera designs employ only even-order surfaces.[14–16] Tanikawa et al.[4] first introduced odd-order surfaces and demonstrated the effectiveness in aberration correction. Since higher-order gradients of odd-order surfaces are undefined at the origin, the surface figure cannot be intrinsically expanded as the form of the even-order power series. Therefore, the associated wavefront aberrations cannot be expanded, and thus it is impossible to define aberration coefficients at the origin. Such wavefront aberration cannot be allowed for precision optics. To avoid this, we apply odd-order terms into only

*Address all correspondence to: Takao Tanabe, E-mail: tanabe-t@hakuto.co.jp

the surfaces annular in shape in this paper. As a result, we obtain a much improved design that is allowable for up-to-date lithography tools. In this case, as predicted by the theoretical analysis in Sec. 2, odd-order surfaces are specifically effective in correcting higher-order coma, astigmatism, and tetrafoil. Moreover, the required number of even-order terms that sufficiently approximates odd-order shape is not realistic. From these two reasons, we conclude that odd-order surfaces provide a new degree of freedom in lens optimization.

2 Derivation of Wavefront Aberration Coefficients of Odd-Order Surfaces

2.1 *Wavefront Seidel Aberrations for Spherical Surfaces*

Deriving aberration coefficients involves expanding a wavefront function into power series.[7–13] In this paper, following the method of Conrady,[7] we derive aberration coefficients by using the optical path differences (OPD) between a ray and the principal ray. This method is easily applied to not only conventional even-order surfaces but also any aspherical surfaces.

Figure 1 illustrates the optical relation of the object, the entrance pupil, the exit pupil, and the image in a lens system. For simplicity, the height of the marginal ray at the exit pupil is normalized to unity. This normalization simplifies the ray coordinate.

Expanding the wavefront function into power series of normalized pupil coordinates (ξ, η) provides wavefront aberration coefficients of a single surface. According to Shack's notation,[13] the wavefront function of an ordinary rotational system is expanded as

$$W(\xi,\eta;h) = W_{000} + W_{200}h^2 + W_{111}h\eta + W_{020}(\xi^2+\eta^2) + W_{040}(\xi^2+\eta^2)^2 + W_{131}h\eta(\xi^2+\eta^2) + W_{222}h^2\eta^2 + W_{220}h^2(\xi^2+\eta^2) + W_{311}h^3\eta + \cdots, \quad (1)$$

where h means the relative (normalized) image height that lies along y-axis. Also, W_{ijk} are the wavefront aberration coefficients and have the unit of length. In this equation, we implicitly assume that there is rotational symmetry of the optical system and the possibility of Taylor expansion for any system functions, such as surface figure and wavefront aberration.

In Eq. (1), the first four coefficients $W_{000}, W_{200}, W_{111}$, and W_{020} correspond to the constant piston, the field-dependent piston (the difference between the optical path length of an on-axis ray and that of extra-axial principal ray), the magnification error, and defocus, respectively. The fourth-order coefficients $W_{040}, W_{131}, W_{222}, W_{220}$, and W_{311} represent Seidel aberrations and correspond to spherical aberration, coma, astigmatism, field curvature, and distortion, respectively. These five wavefront errors dominantly affect the image quality and thus they are the first target to be corrected.

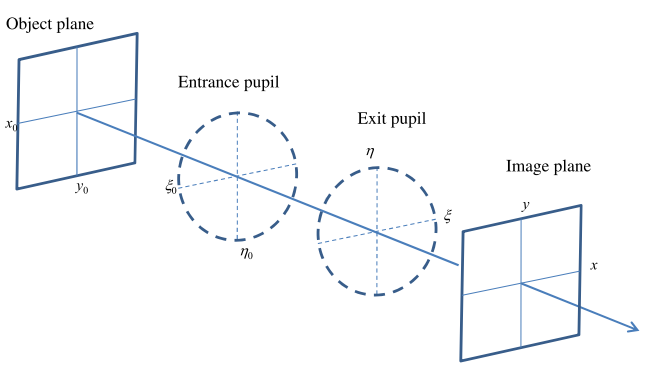

Fig. 1 Definition of coordinate system for analyzing aberrations.

2.2 *Wavefront Aberrations Induced by Small Asphericity*

In this section, we represent the aspherical contributions of narrow bundles along the principal ray for rotationally symmetric optical systems. If the asphericity is small, the optical path induced by the aspherical sag simply corresponds to the additional wavefront aberration. We consider a sphere-based aspherical surface, which is denoted as

$$z = \frac{cr^2}{1+\sqrt{1-c^2r^2}} + f(X,Y), \quad (2)$$

where c is the curvature of the base sphere, (X, Y) is the coordinate on the tangent plane at the vertex, the radial coordinate $r^2 = X^2 + Y^2$, and $f(X, Y)$ is a small asphericity from the base sphere.

Since the intersection point between an incident ray and aspherical surface cannot be analytically derived, an iterative method is employed in practical ray tracing for the aspherical surface. In the meridional section, Fig. 2 shows an incident meridional ray from air to the material refracting at point P on an aspherical surface.

Generally, the lowest order approximation of the aspherical sag from the base sphere provides the additional optical path of an incident skew ray

$$[P_0P] \sim [P_0P_1] = z_0 \cos\theta = f(X_0,Y_0)\cos\theta, \quad (3)$$

where $\cos\theta$ denotes the direction cosine of the incident ray along the z-axis and (X_0, Y_0) is the coordinate of the incident point P_0 projected onto the tangent plane at the vertex. Owing to the normalization of pupil coordinates, the incident point (X_0, Y_0) is referred to the normalized pupil coordinate (ξ, η) as

$$(X_0, Y_0) = (y\xi, y\eta + \bar{y}), \quad (4)$$

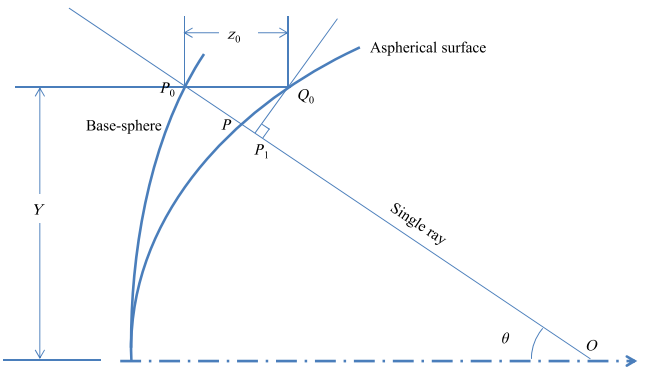

Fig. 2 Ray tracing at an aspherical surface of a single ray in the meridional plane.

where y and $\bar{y}$ correspond to the actual paraxial marginal and actual paraxial principal ray height, respectively. Note that while the image height h, which appears in Eq. (1), is normalized by the marginal image height and the $\bar{y}$ is the actual principal ray height.

By considering not only an incident skew ray but also an exit skew ray from the surface, the wavefront aberration function $W(\xi,\eta;\bar{y})$, which corresponds to the OPD between a ray and the principal ray, is represented as follows:

$$W(\xi,\eta;\bar{y}) = (n\cos\theta' - \cos\theta)[f(y\xi, y\eta+\bar{y}) - f(0,\bar{y})], \tag{5}$$

where n is the index of the material and $\cos\theta'$ denotes the direction cosine of the exit ray along the z-axis.

By applying the Taylor series of $f(X,Y)$ to Eq. (5)

$$\begin{aligned} W(\xi,\eta;\bar{y}) &= (n\cos\theta' - \cos\theta) \\ &\times\left\{ y\left(\frac{\partial f}{\partial X}\xi + \frac{\partial f}{\partial Y}\eta\right) + \frac{y^2}{2}\left(\frac{\partial^2 f}{\partial X^2}\xi^2 + 2\frac{\partial^2 f}{\partial X\partial Y}\xi\eta + \frac{\partial^2 f}{\partial Y^2}\eta^2\right)\right. \\ &+ \frac{y^3}{3!}\left(\frac{\partial^3 f}{\partial X^3}\xi^3 + 3\frac{\partial^3 f}{\partial X^2\partial Y}\xi^2\eta + 3\frac{\partial^3 f}{\partial X\partial Y^2}\xi\eta^2 + \frac{\partial^3 f}{\partial Y^3}\eta^3\right) \\ &+ \frac{y^4}{4!}\left(\frac{\partial^4 f}{\partial X^4}\xi^4 + 4\frac{\partial^4 f}{\partial X^3\partial Y}\xi^3\eta + 6\frac{\partial^4 f}{\partial X^2\partial Y^2}\xi^2\eta^2\right. \\ &\left.\left. + 4\frac{\partial^4 f}{\partial X\partial Y^3}\xi\eta^3 + \frac{\partial^4 f}{\partial Y^4}\right) + \cdots\right\}, \end{aligned} \tag{6}$$

where each derivative $\frac{\partial^{m+n} f}{\partial X^m \partial Y^n}$ means $\frac{\partial^{m+n} f}{\partial X^m \partial Y^n}(0,\bar{y})$. This formulation is the basis to derive wavefront aberration coefficients.

2.3 *Aberration Coefficients of Odd-Order Aspherical Surfaces*

We demonstrate the derivation of aberration coefficients of the second- and fourth-order aspherical surfaces. These surfaces assume a major role in Seidel aberration theory. The second-order aspherical surface is represented by the simple quadric form. Namely

$$f(X,Y) = A(X^2+Y^2), \tag{7}$$

where A is the aspherical coefficient. By substituting Eq. (7) into Eq. (5), the aberration coefficients are calculated as

$$\begin{aligned} W(\xi,\eta;\bar{y}) &= A(n-1)\cos\theta[(y\xi)^2 + (y\eta+\bar{y})^2 - \bar{y}^2] \\ &= A(n-1)\cos\theta[y^2(\xi^2+\eta^2) + 2y\bar{y}\eta]. \end{aligned} \tag{8}$$

In this expression, the first term represents the power added to the base surface shape. The second term is the wavefront tilt that means a magnification error. The fourth-order surface is also represented as

$$f(X,Y) = A(X^2+Y^2)^2, \tag{9}$$

where A is the fourth-order aspherical coefficient. The wavefront function in Eq. (5) is

$$\begin{aligned} W(\xi,\eta;\bar{y}) &= A(n-1)\cos\theta\times[4y\bar{y}^3\eta + 2y^2\bar{y}^2(\xi^2+3\eta^2) \\ &+ 3y^3\bar{y}\eta(\xi^2+\eta^2) + y^4(\xi^2+\eta^2)^2]. \end{aligned} \tag{10}$$

The above equation represents Seidel aberration coefficients of a fourth-order surface: distortion, astigmatism, coma, and spherical aberrations, respectively. Note that dividing the second term into astigmatism and field curvature is possible.

The method described above enables the calculation of aberration coefficients for any aspherical surfaces. We derive explicit expressions for the first- and third-order surfaces, which will be applied to the extreme ultraviolet (EUV) optical design described in Sec. 3.

Odd-order aspherical surfaces are expressed by the polynomial to the odd powers of r, which become half-integer powers of $r = X^2+Y^2$. The first-order aspherical surface is given by $f(X,Y) = A(X^2+Y^2)^{1/2}$ and the third-order aspherical surface is given by $f(X,Y) = A(X^2+Y^2)^{3/2}$. For both surfaces, the higher-order derivatives $\frac{\partial^{m+n} f}{\partial X^m \partial Y^n}(0,\bar{y})$ do not vanish. Thus, the wavefront expression of Eq. (8) contains an infinite number of terms. Namely

$$\begin{aligned} W(\xi,\eta) &= A(n-1)\cos\theta\times\left[y\eta + \frac{y^2}{2\bar{y}}\times\xi^2 - \frac{y^3}{2\bar{y}^2}\right. \\ &\left.\times\xi^2\eta - \frac{y^4}{8\bar{y}^3}\times(\xi^4 - 4\xi^2\eta^2) + \cdots\right], \end{aligned} \tag{11}$$

for the first-order aspherical surface and

$$\begin{aligned} W(\xi,\eta) &= A(n-1)\cos\theta\times\left[3y\bar{y}^2\eta + \frac{3y^2\bar{y}}{2}(\xi^2+2\eta^2)\right. \\ &\left. + \frac{y^3}{2}\eta(3\xi^2+2\eta^2) + \frac{3y^4}{8y}\times\xi^4\ \cdots\right], \end{aligned} \tag{12}$$

for the third-order aspherical surface.

By classifing terms in Eqs. (11) and (12) by the order of pupil coordinates, Table 1 represents the aberration components of the first-, second-, third- and fourth-order aspherical surfaces.

The ordinary even-order aspherical surfaces, which are the second- and fourth-order aspherical surface in this table, correspond to Gaussian optics and Seidel aberration theory. However, the aberration coefficients of odd-order aspherical surfaces are completely different from those of the fourth-order aspherical surface. For example, similar to astigmatism, the y^4 aberration coefficients of odd-order surfaces are not rotationally invariant while that of the fourth-order surface is just Seidel spherical aberration and rotationally invariant. The y^4 aberration coefficient of the first-order aspherical surface is decomposed by Zernike polynomials as

$$\begin{aligned} W &= \xi^4 - 4\xi^2\eta^2 = \frac{\rho^4}{8}(5\cos 4\phi + 4\cos 2\phi - 1) \\ &= \frac{1}{8}(5Z_{17} + Z_{12} - 3Z_5 - 1), \end{aligned} \tag{13}$$

where $\xi = \rho\cos\phi$ and $\eta = \rho\sin\phi$ in the pupil plane. The classification of Zernike polynomials used in Eq. (13) is shown in Table 2.

Table 1 Wavefront aberration coefficients of up to the fourth-order aspherical surface.

Power of y	First-order aspherical surface	Second-order aspherical surface	Third-order aspherical surface	Fourth-order aspherical surface
y	$y\eta$	$2y\bar{y}\eta$ (magnification error)	$3y\bar{y}^2\eta$	$4y\bar{y}^3\eta$ (distortion)
y^2	$\frac{y^2}{2\bar{y}}\times\xi^2$	$y^2(\xi^2+\eta^2)$ (defocus)	$\frac{3y^2\bar{y}}{2}(\xi^2+2\eta^2)$	$2y^2\bar{y}^2\times(\xi^2+3\eta^2)$ (astigmatism)
y^3	$-\frac{y^3}{2\bar{y}^2}\times\xi^2\eta$	0	$\frac{y^3}{2}\eta(3\xi^2+2\eta^2)$	$3y^3\bar{y}\times\eta(\xi^2+\eta^2)$ (coma)
y^4	$-\frac{y^4}{8\bar{y}}\times(\xi^4-4\xi^2\eta^2)$	0	$\frac{3y^4}{8\bar{y}}\times\xi^4$	$y^4\times(\xi^2+\eta^2)^2$ (spherical)

Table 2 Classification of Zernike polynomials used in Eq. (13).

Expressions of Zernike polynomials	Classification
$Z_{17}=\rho^4\cos 4\phi$	Tetra-foil
$Z_{12}=(4\rho^4-3\rho^2)\cos 2\phi$	Sixth-order astigmatism
$Z_5=\rho^2\cos 2\phi$	Seidel astigmatism

This expression represents that the y^4 aberration coefficient of the first-order aspherical surface is the combination of tetrafoil, sixth-order astigmatism, and Seidel astigmatism. As Eq. (13), the y^4 aberration coefficient of the third-order aspherical surface $W=\xi^4$ also consists of the nonrotational Zernike polynomials in Table 2

$$W=\xi^4=\frac{\rho^4}{8}(\cos 4\phi+4\cos 2\phi+3)$$
$$=\frac{1}{8}(Z_{17}+Z_{12}-3Z_5+3). \quad (14)$$

From this point of view, the odd-order aspherical surfaces, which are considered as low-order aspherical surface, are effective in aberration correction because their aberration coefficients contain higher-order Zernike polynomials, such as Z_5, Z_{12}, and Z_{17}.

3 Design Application

3.1 *Outline of Optical Design*

Since the beginning of 1990s, optical designs of EUVL cameras have been researched extensively. Since no refractive material is available for EUV region, all EUV optical systems are designed with mirrors. Among them a six-mirror configuration that includes one pupil relay is optimal for the balance between the field width and nonobscured numerical aperture. All optical surfaces are rotationally symmetrical around the common axis. However, the aperture of each surface is decentered, and the axial point is not imaged by the system. Figure 3 illustrates the basic configuration of six-mirror EUVL projection system.

The system in Fig. 3 consists of three groups. The reticle side group (M1 and M2) reduces the angle of rays that enter the pupil relay group (M3 and M4) in order to correct the extra-axial ray aberrations. The aperture stop is placed at M2. The pupil relay group (M3 and M4) makes the image of the aperture stop onto M5, which is placed in the wafer side group. Also, the intermediate reticle image is formed between M4 and M5. The wafer side group resembles the reticle side group.

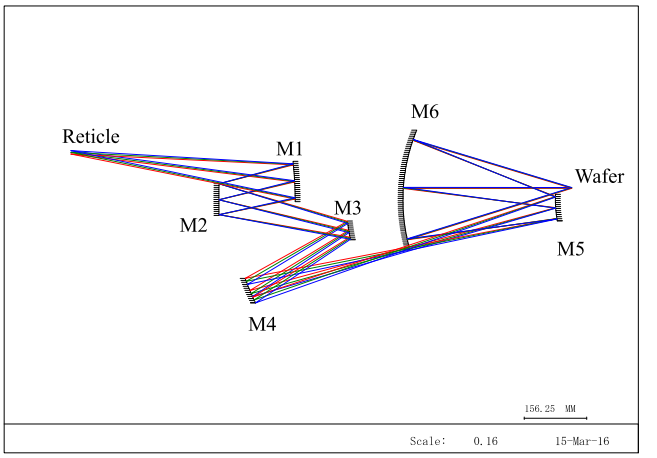

Fig. 3 Basic configuration of six-mirror EUVL projection system.

In this section, we describe two designs of this six-mirror EUVL camera to disclose the effectiveness of odd-order aspherical surfaces. One is designed with only even-order aspherical terms and the other with additional odd-order terms. Table 3 represents the optical design specifications:

In optical design, the merit function is constructed so that the real magnification and real telecentricity are constrained only in the exposure field, that is, this optical system does not necessarily satisfy these specifications in the sense of paraxial optics. Further, the merit function based on wavefront aberrations with Gaussian quadrature is suitable for such a

Table 3 Optical design specifications for EUVL camera.

Features	Specifications
Wavelength	13.5 nm
Numerical aperture	0.3 on wafer side
Exposure field	$Y'=28.5$ to 30.5 (2-mm slit)
Magnification	−1/4
Telecentricity	Telecentric at wafer plane
Residual wavefront aberration	Less than 0.006λ; (Strehl ratio >0.998)

Table 4 EUVL projection system with only aspherical even-order terms.

	Radius of curvature	Thickness	Material
Object	Infinity	560.8785	
1	−820.9470	−190.176	Reflective
2*	2206.467	319.2278	Reflective
3	474.5155	−287.472	Reflective
4	573.4281	810.925	Reflective
5	286.7007	−381.439	Reflective
6	453.9792	422.1489	Reflective
Image	Infinity		

Surface no.	1	2	3	4	5	6
Normalization radius	90	40.5	100	257.5	48.5	150
A1	0	0	0	0	0	0
A2	0	0	0	0	0	0
A3	0	0	0	0	0	0
A4	2.232809×10^{-01}	$-2.881597 \times 10^{-03}$	$-2.152907 \times 10^{-01}$	$-9.832075 \times 10^{-02}$	$-2.395010 \times 10^{-03}$	3.696353×10^{-02}
A5	0	0	0	0	0	0
A6	$-4.772316 \times 10^{-02}$	$-3.131182 \times 10^{-04}$	6.599907×10^{-03}	1.272619×10^{-02}	2.296908×10^{-02}	5.349752×10^{-03}
A7	0	0	0	0	0	0
A8	1.286259×10^{-02}	$-3.977065 \times 10^{-05}$	1.192252×10^{-03}	$-2.210501 \times 10^{-02}$	$-3.021419 \times 10^{-03}$	6.579361×10^{-04}
A9	0	0	0	0	0	0
A10	$-3.111194 \times 10^{-03}$	$-3.388733 \times 10^{-06}$	$-1.066165 \times 10^{-03}$	1.081757×10^{-02}	5.460242×10^{-04}	7.172373×10^{-05}
A11	0	0	0	0	0	0
A12	4.695752×10^{-04}	0	2.058089×10^{-04}	$-1.694801 \times 10^{-03}$	$-1.072324 \times 10^{-04}$	1.554783×10^{-05}

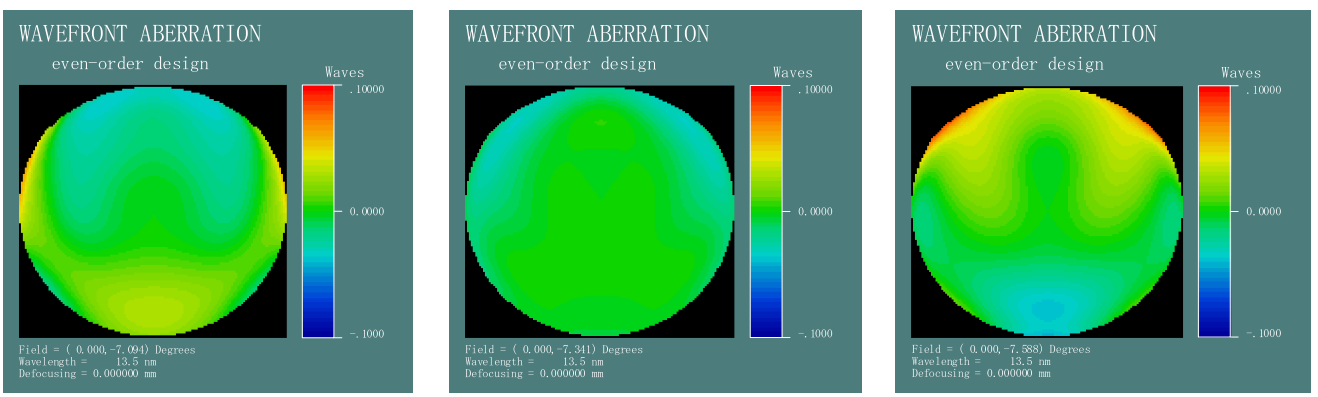

(a) (b) (c)

Fig. 4 Wavefront aberration of the even-order design: (a) bottom, (b) center, and (c) top.

Table 5 Zernike decomposition of the wavefront aberrations of even-order design (units are in waves).

Coma			
Field	Bottom	Center	Top
Z_8	−0.0045	0.0068	−0.0038
Z_{15}	−0.0099	0.0013	0.0065
Z_{24}	0.0005	−0.0021	−0.0054
Z_{35}	−0.0013	−0.0018	−0.0023
Astigmatism			
Field	Bottom	Center	Top
Z_5	0.0031	−0.0052	0.0017
Z_{12}	0.0174	0.0026	−0.0182
Z_{21}	−0.0029	0.0006	0.0057
Z_{32}	−0.0023	−0.0019	−0.0012
Trefoil			
Field	Bottom	Center	Top
Z_{11}	−0.0070	0.0087	−0.0030
Z_{20}	−0.0073	−0.0026	0.0063
Z_{31}	−0.0030	−0.0029	−0.0025
Tetrafoil			
Field	Bottom	Center	Top
Z_{17}	0.0124	0.0019	−0.0211
Z_{28}	0.0007	0.0008	0.0004

highly corrected optical system. All designs are achieved with Code-V™. The radii of base spheres, the air spaces, and the aspherical coefficients (excluding the conic constant) are chosen for optimization.

3.2 *Design with Even-Order Aspherical Terms*

Table 4 represents a conventional EUVL system that is designed with only sphere-based even-order aspherical terms.

In this design, the aperture stop is placed on the second surface that is indicated by the asterisk. The aspherical surface shapes are described by the following equation:

$$z = \frac{cr^2}{1 + \sqrt{1 - c^2 r^2}} + \sum_{n=1}^{12} A_n \rho^n, \tag{15}$$

where c is the curvature of the base sphere, r is the radial coordinate, and ρ is the normalized radial coordinate of which normalization radius is indicated in Table 4. To meet the specification, even-order aspherical terms up to 12th order are needed. However, the Strehl ratios of this design are at the level of 0.995, which are not sufficient for up-to-date lithography tools.[17] As we have practically confirmed by a study of lens design, the use of even-order aspherical coefficients up to 30th-, the second-order term, and the conic coefficient has little effect on wavefront improvement in this case. We infer that the ineffectiveness of the second order is based on the fact that the second-order aspherical term only generates the power and magnification error that do not involve the higher-order aberrations. Also, since the conic constant can be closely represented by ordinary even-order aspherical surface, it does not improve the optical performance significantly.

Figure 4 shows the wavefront aberration of the bottom, center, and top of the field. Note that the scale is $-\lambda/10$ to $+\lambda/10$. The residual root-mean-square (RMS) wavefronts are 0.012, 0.008, 0.011 waves, respectively. Also the Strehl ratio is 0.995, 0.997, and 0.996.

Table 5 and Fig. 5 show the Zernike decomposition of the wavefront aberrations. The strong asymmetry in the pupil

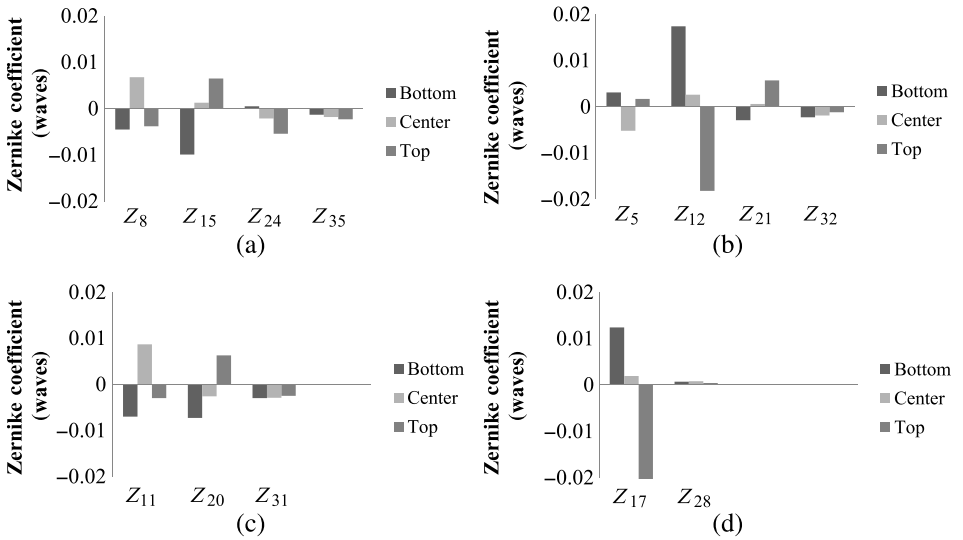

Fig. 5 Bar diagrams of the Zernike coefficients described in Table 5. (a) Coma, (b) astigmatism, (c) trefoil, and (d) tetrafoil.

relay (M3 and M4), which come from the large decentering, causes asymmetrical aberrations, such as tilt, coma, and astigmatism. Although the Seidel aberrations (Z_8 for coma and Z_5 for astigmatism) are well-corrected, the sixth-order wavefront aberrations (Z_{15}, Z_{12}, and Z_{17}) are large and their signs at the top of the fields are opposite to those at the bottom. Among them, sixth-order astigmatism (Z_{12}) and tetrafoil (Z_{17}) are dominant.

3.3 *Improvement by Utilizing Odd-Order Aspherical Terms*

As shown in Sec. 2, odd-order aspherical surfaces have the capability to control sixth-order wavefront aberrations (Z_{12} and Z_{17}) independently. Introducing odd-order aspherical terms into M3 and M4 reduces the residual wavefront aberration significantly. Table 6 shows an optical design form with odd-order aspherical terms.

Table 7 compares the residual RMS wavefront of even-order design and that of the design using both even- and odd-order terms. In the design with odd-order terms, the Strehl ratios over the entire exposure field are almost 0.999 as required for up-to-date lithography tools.[17] Figure 6 shows the wavefront aberrations of the bottom, center, and top of the field. The scale is the same as Fig. 4.

Table 7 Comparison of residual RMS wavefront of two designs (units are in waves).

	Bottom	Center	Top
Only even-order	0.0116	0.008	0.0105
Both even- and odd-order	0.0058	0.0056	0.0054

Table 8 and Fig. 7 show the Zernike decomposition of the wavefront aberrations. By comparing Tables 5 and 8, the use of odd-order aspherical terms in M3 and M4 does not change the balance of Seidel aberrations of coma (Z_8) and astigmatism (Z_5). The sixth-order astigmatism (Z_{12})

Table 6 EUVL projection system with odd-order aspherical terms.

	Radius of curvature	Thickness	Material
Object	Infinity	573.3432	
1	−839.4372	−200.5083	reflective
2*	1945.2131	353.6812	reflective
3	529.8170	−288.8153	reflective
4	584.2007	857.2901	reflective
5	281.1104	−376.3534	reflective
6	454.4199	423.0405	reflective
Image	Infinity		

Surface no.	1	2	3	4	5	6
Normalization radius	91.5	40.5	103	262	48	150
A1	0	0	2.025075×10^{-01}	$-5.005588 \times 10^{-01}$	0	0
A2	0	0	0	0	0	0
A3	0	0	1.015068×10^{00}	$-5.603777 \times 10^{-01}$	0	0
A4	2.359900×10^{-01}	$-2.580754 \times 10^{-03}$	$-9.049848 \times 10^{-01}$	$-2.558581 \times 10^{-01}$	$-3.623837 \times 10^{-03}$	3.862932×10^{-02}
A5	0	0	4.549866×10^{-02}	$-4.558530 \times 10^{-02}$	0	0
A6	$-3.896598 \times 10^{-02}$	$-2.214112 \times 10^{-04}$	1.561940×10^{-01}	1.008751×10^{-01}	1.514787×10^{-02}	5.490149×10^{-03}
A7	0	0	5.883905×10^{-02}	9.252107×10^{-02}	0	0
A8	8.224229×10^{-03}	$-3.315761 \times 10^{-05}$	$-4.329746 \times 10^{-02}$	7.071586×10^{-04}	$-1.313364 \times 10^{-03}$	6.231698×10^{-04}
A9	0	0	$-6.664260 \times 10^{-02}$	$-9.514685 \times 10^{-02}$	0	0
A10	$-1.684451 \times 10^{-03}$	0	1.680247×10^{-03}	$-6.676155 \times 10^{-02}$	2.858667×10^{-04}	1.114371×10^{-04}
A11	0	0	5.288878×10^{-02}	8.182442×10^{-02}	0	0
A12	2.327812×10^{-04}	0	$-2.077366 \times 10^{-02}$	$-1.109241 \times 10^{-02}$	$-7.407131 \times 10^{-05}$	0

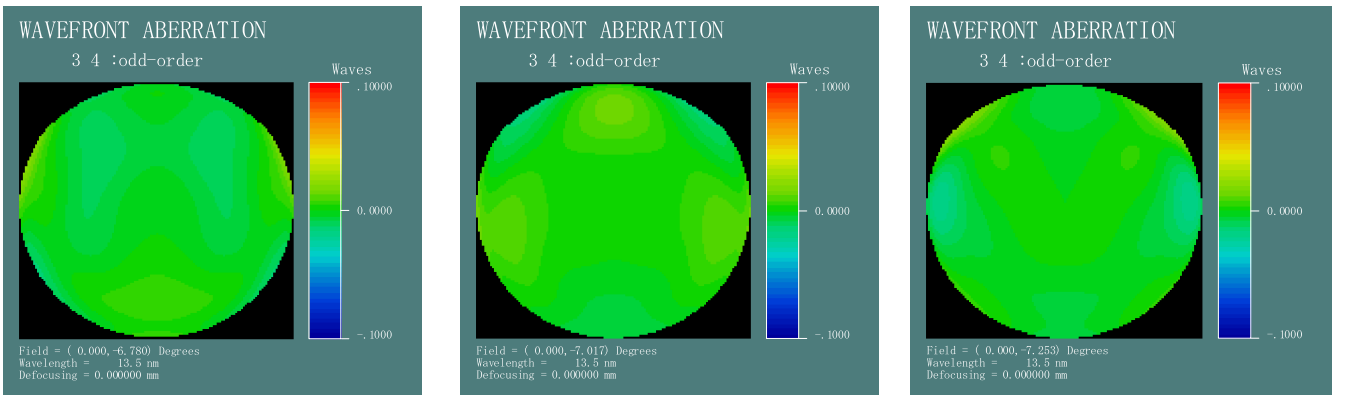

(a) (b) (c)

Fig. 6 Wavefront aberration of the odd-order design: (a) bottom, (b) center, and (c) top.

Table 8 Zernike decomposition of the wavefront aberrations of the design with odd-order terms (units are in waves)

Coma			
Field	Bottom	Center	Top
Z_8	−0.0044	0.0036	0.0005
Z_{15}	−0.0020	0.0033	−0.0002
Z_{24}	0.0008	−0.0012	−0.0023
Z_{35}	0.0000	−0.0002	−0.0003
Astigmatism			
Field	Bottom	Center	Top
Z_5	−0.0011	0.0046	−0.0035
Z_{12}	0.0045	0.0004	−0.0031
Z_{21}	−0.0023	0.0002	0.0010
Z_{32}	−0.0003	0.0002	0.0007
Trefoil			
Field	Bottom	Center	Top
Z_{11}	−0.0034	0.009	−0.0017
Z_{20}	−0.0026	−0.0020	0.0030
Z_{31}	−0.0020	−0.0013	−0.0017
Tetrafoil			
Field	Bottom	Center	Top
Z_{17}	0.0046	0.0059	−0.0119
Z_{28}	−0.0010	−0.0016	0.0004

and tetrafoil (Z_{17}) are evidently reduced, while lower-order trefoil (Z_{11}) still remains. Also, sixth-order coma (Z_{15}) is reduced.

In Sec. 2.3, we have proven that the y^4 aberration coefficients, which correspond to spherical aberration for ordinary fourth-order aspherical term, of the first- and the third-order aspherical surfaces contain tetrafoil (Z_{17}) and the sixth-order astigmatism (Z_{12}). Hence, odd-order surfaces have stronger capabilities of correcting nonsymmetrical aberrations than even-order surfaces, as shown in this design example.

3.4 *Practical Impossibility of Expansion of Odd-Order Aspherical Terms into Even-Order Power Series*

Tanabe et al.[6] have derived the expansion formula for monomial and described the possibility of the close approximation of odd-order aspherical terms by a finite number of even-order aspherical terms. As proven in Ref. 6, the Zernike expansion of monomial t^α is given as

$$t^\alpha = \sum_{n=0}^{\infty} a_n Q_n(t) = \sum_{n=0}^{\infty} \frac{(2n+1)\Gamma(\alpha+1)^2}{\Gamma(\alpha+n+2)\Gamma(\alpha-n+1)} Q_n(t), \tag{16}$$

where $\Gamma(x)$ is the gamma function and $Q_n(t) = \frac{(-1)^n}{n!}\frac{d^n}{dt^n} t^n(1-t)^n$, which correspond to rotationally symmetric Zernike polynomials. The variable t is the square of the normalized pupil coordinate, that is, $t = r^2$.

In practical lens design, the number of available aspherical coefficients is realistically finite. For example, the maximum order of "odd-order asphere" in Code-V is limited to the 30th-order coefficients. "extended odd asphere" in Zemax allows 240 aspherical coefficients. However, such an extremely high-order coefficient is not practically meaningful in optical design.

Table 9 represents the even-order expansion coefficients of odd-order aspherical surfaces up to 11th that were used in the practical design described in Sec. 3.3. Note that the radial coordinate r is used instead of $t = r^2$ and this is directly derived from Eq. (16). All odd-order aspherical surfaces are expanded by rotationally invariant Zernike polynomials (powers of radius are up to 30th) and then rearranged to the conventional even-order polynomial up to the 30th order, the actual upper limit of Code-V. This table shows

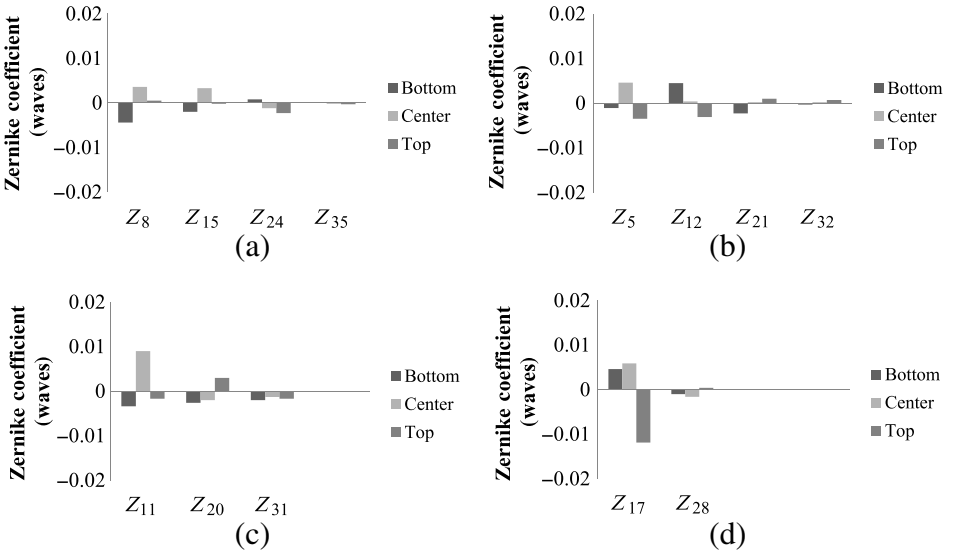

Fig. 7 Bar diagrams of the Zernike coefficients described in Table 8. (a) Coma, (b) astigmatism, (c) trefoil, and (d) tetraoil.

that the expansion coefficients of lower odd-order surfaces contain very large positive and negative values. For the first-order surface, the coefficients over 12th are 1E6 or 1E7 order in absolute value. The impossibility of expansion of odd-order surfaces into even-order power series leads to such diverging and vibrating expansion coefficients.

By using Table 9, one obtains even-order polynomials that approximate the odd-order aspherical mirror shapes (M3 and M4). Figure 8 shows the approximation error of M3 for example. The effective apertures of such mirrors are annular in shape, and the minimum normalized radii are larger than at least 0.8.

Table 9 Coefficients of even-order aspherical terms for approximating odd-order aspherical surfaces.

n	r	r^3	r^5	r^7	r^9	r^{11}
0	3.128055×10^{-02}	-9.245482×10^{-05}	1.388211×10^{-06}	-4.983320×10^{-08}	3.329260×10^{-09}	-3.650024×10^{-10}
2	7.976540×10^{00}	7.072794×10^{-02}	-5.899895×10^{-04}	1.779045×10^{-05}	-1.091521×10^{-06}	1.137589×10^{-07}
4	-1.675073×10^{02}	4.455860×10^{00}	1.115080×10^{-01}	-1.867997×10^{-03}	9.627219×10^{-05}	-9.214472×10^{-06}
6	2.758287×10^{03}	-4.076287×10^{01}	3.060275×10^{00}	1.537985×10^{-01}	-4.403561×10^{-03}	3.540405×10^{-04}
8	-2.955308×10^{04}	3.668658×10^{02}	-1.530138×10^{01}	2.306977×10^{00}	1.981603×10^{-01}	-8.851012×10^{-03}
10	2.123881×10^{05}	-2.421314×10^{03}	8.483083×10^{01}	-7.105489×10^{00}	1.831001×10^{00}	2.453500×10^{-01}
12	-1.061941×10^{06}	1.150872×10^{04}	-3.702933×10^{02}	2.605346×10^{01}	-3.729816×10^{00}	1.499361×10^{00}
14	3.795979×10^{06}	-3.977874×10^{04}	1.216678×10^{03}	-7.861612×10^{01}	9.453943×10^{00}	-2.111346×10^{00}
16	-9.869546×10^{06}	1.009768×10^{05}	-2.986392×10^{03}	1.834376×10^{02}	-2.025845×10^{01}	3.800422×10^{00}
18	1.881449×10^{07}	-1.890718×10^{05}	5.459453×10^{03}	-3.242584×10^{02}	3.404197×10^{01}	-5.864849×10^{00}
20	-2.626107×10^{07}	2.602517×10^{05}	-7.381180×10^{03}	4.280211×10^{02}	-4.344994×10^{01}	7.116017×10^{00}
22	2.650911×10^{07}	-2.597989×10^{05}	7.266354×10^{03}	-4.138716×10^{02}	4.101917×10^{01}	-6.495838×10^{00}
24	-1.882531×10^{07}	1.828215×10^{05}	-5.056702×10^{03}	2.840296×10^{02}	-2.764996×10^{01}	4.275039×10^{00}
26	8.915846×10^{06}	-8.593126×10^{04}	2.355235×10^{03}	-1.308252×10^{02}	1.255941×10^{01}	-1.907325×10^{00}
28	-2.527167×10^{06}	2.420105×10^{04}	-6.582955×10^{02}	3.623438×10^{01}	-3.440012×10^{00}	5.151838×10^{-01}
30	3.241745×10^{05}	-3.087377×10^{03}	8.344261×10^{01}	-4.558181×10^{00}	4.288184×10^{-01}	-6.350921×10^{-02}

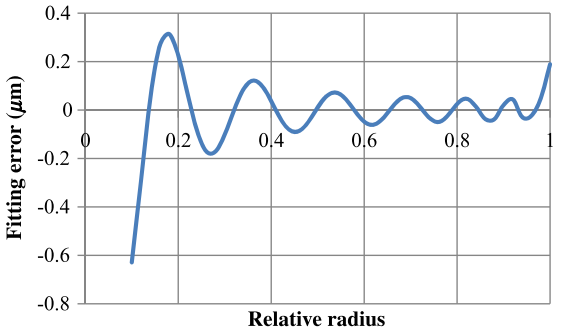

Fig. 8 Approximation error of M3 via using the expansion described in Table 9.

By this approximation, the resultant wavefront errors of total optical system are represented in Fig. 9. This result shows that the expansion of odd-order surfaces into even-order power series does not work well in extreme short wavelength region, even though we use the maximum number of terms in Code-V. Actually, the wavefront errors exceed 10λ that cannot be accepted in high-performance optics at all. Thus, we conclude that the odd-order surfaces have unique characteristics for aberration correction and provide degrees of freedom in optical design.

In addition, as argued in Sec. 2.3, odd-order aspherical surfaces are effective in correcting higher-order aberrations of extra-axial image points. Thus, we note that odd-order aspherical surfaces are also valuable in optical designs, such as highly decentered or tilted projection display optics, head-up displays, and infrared all-reflective systems.

4 Summary

We have theoretically investigated the aberration properties of odd-order aspherical surfaces and reported an application of odd-order aspherical surfaces for concrete optical design of EUVL cameras. By constructing aberration theory for odd-order aspherical surfaces, we have analytically described the extra-axial wavefront aberrations induced by them. This theory is based on Taylor expansion of wavefront aberration function induced by the aspherical deviation from the base sphere. By this analysis, we disclosed that aberration coefficients of low odd-order aspherical surfaces contain higher-order aberrations, such as astigmatism and tetrafoil, Thus, we theoretically predicted that odd-order aspherical surfaces are effective in aberration correction.

In design application for EUVL cameras, we confirmed that odd-order aspherical surfaces are effective for correcting higher-order aberrataions. Moreover, we confirmed that these odd-order aspherical surfaces are not exactly represented by the realisitc number of even-order terms. Hence, we have concluded that odd-order aspherical surfaces provide degree of freedom in aberration correction and are practically effective at least for high precision and short exposure wavelength optics.

Referring to the theoretical investigations for aberration property of odd-order surface and the design studies of EUVL optics, odd-order aspherical surfaces are effective in correcting higher-order aberrations for extra-axial points because the associated wavefront functions contain higher-order aberrations. Thus odd-order aspherical surfaces are valuable in optical design of not only the EUVL example described here but also highly tilted or decentered optics, such as projection display optics, head-up displays, and all-reflective infrared systems.

Acknowledgments

We would like to thank Mr. Makoto Fujino and Mr. James Webb for their valuable suggestions for completing and refining this paper.

References

1. W. T. Plummer, "Viewfinder for a reflex camera," U.S. Patent No. 3,810,221 (1974).
2. M. Amano, "Projection optical system and projection display apparatus," U.S. Patent No. 8,967,812 (2015).
3. K. Sato, "Wide angle zoom lens including at least one aspheric lens surface," U.S. Patent No. 6,982,834 (2006).
4. M. Tanikawa et al., "Effectiveness of odd order aspherical surface," *Jpn. J. Opt.* **36**(11), 646–660 (2007) (in Japanese).
5. M. Shibuya et al., "Theoretical investigation of the meaning of odd-order aspherical surface and numerical confirmation of effectiveness in rotational-symmetric but off-axis optics," *Opt. Eng.* **49**(7), 073003 (2010).

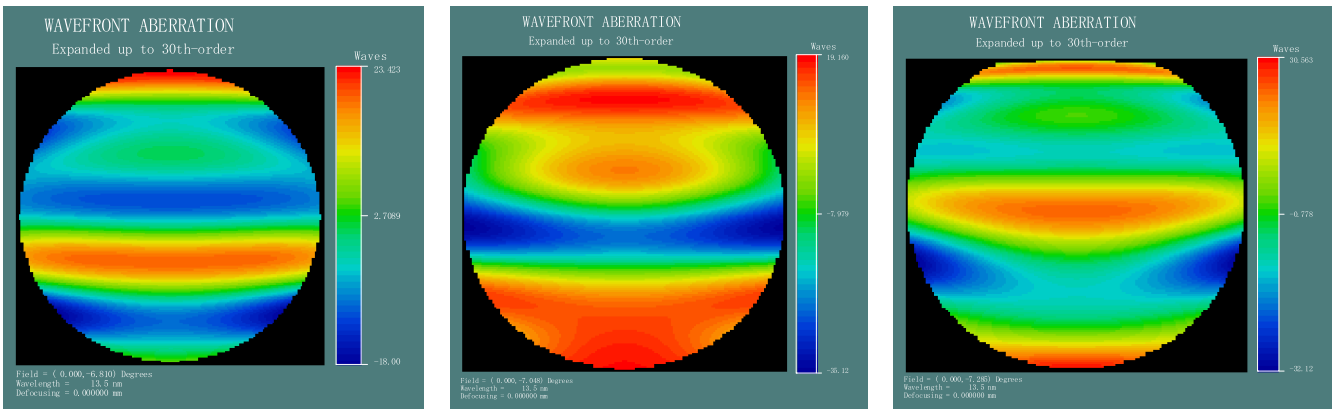

(a) (b) (c)

Fig. 9 Residual wavefront aberrations with expanded shape of M3 and M4: (a) bottom, (b) center, and (c) top.

6. T. Tanabe et al., "Convergence and differentiation of Zernike expansion: application for an analysis of odd-order surfaces," *Opt. Eng.* **55**(3), 035101 (2016).
7. A. E. Conrady, *Applied Optics and Optical Design Part I and II*, Dover Publications, Inc., New York (1957).
8. H. H. Hopkins, *Wave Theory of Aberrations*, Clarendon Press, London (1950).
9. R. Kingslake, *Lens Design Fundamentals*, Academic Press, New York (1978).
10. M. Herzberger, "Theory of image errors of the fifth order in rotationally symmetrical systems. I," *J. Opt. Soc. Am.* **29**(9), 395–406 (1939).
11. M. Herzberger, *Modern Geometrical Optics*, Interscience Publishers, New York (1958).
12. Y. Matsui and K. Nariai, *Fundamentals of Practical Aberration Theory*, World Scientific Publishing Co. Pte. Ltd., Singapore (1993).
13. J. Sasián, "Theory of sixth-order wave aberrations," *Appl. Opt.* **49**(16), D69–D95 (2010).
14. D. W. Sweeney et al., "EUV optical design for a 100 nm CD imaging system," *Proc. SPIE* **3331**, 2 (1998).
15. S. A. Lerner, J. M. Sasián, and M. R. Descour, "Design approach and comparison of projection cameras for EUV lithography," *Opt. Eng.* **39**(3), 792–802 (2000).
16. Y. Li et al., "Progress of optical design for EUV lithography tools in BIT," in *2014 EUVL Workshop*, http://www.euvlitho.com/2014/P56.pdf (2 February 2016).
17. S. Ishiyama et al., "High-order aberration control during exposure for leading-edge lithography projection optics," *Proc. SPIE* **9780**, 97800Y (2016).

Takao Tanabe is a lens designer at Hakuto Co., Ltd. He received his MS degree in mathematics from Tokyo Institute of Technology in 2005. After an 11-year career in Topcon, he transferred to Hakuto. He has designed lithographic optics, medical optics, and laser optics. He is studying optics at Tokyo Polytechnic University. He is a professional engineer, Japan (mechanical), and also a member of SPIE.

Masato Shibuya is a professor in the Department of Media and Image Technology, Faculty of Engineering, Tokyo Polytechnic University. He graduated from Tokyo Institute of Technology in 1977 with a master's degree in physics and joined Nikon Corporation. He received his PhD from the University of Tokyo in 1996. He joined Tokyo Polytechnic University in 2001, and his research interests include fundamental lens optics, optical lithography, super-resolution, and phase-shifting mask. He is a SPIE fellow.